Aalborg Universitet

A closed-form formulation for the conformal articulation of metal-on-polyethylene hip prostheses

contact mechanics and sliding distance

Renani, Ehsan Askari; Andersen, Michael Skipper

A closed-form formulation for the conformal articulation of metal-on-polyethylene hip prostheses: contact mechanics and sliding distance

Ehsan Askari[1, 1], Michael S. Andersen[1]

[1] Department of Materials and Production, Aalborg University, Aalborg 9220, Denmark

Abstract

Using Hertz contact law results in inaccurate outcomes when applied to the soft conformal hip implants. The finite element method also involves huge computational time and power. In addition, the sliding distance computed using the Euler rotation method does not incorporate tribology of bearing surfaces, contact mechanics and inertia forces. The present study therefore aimed to develop a nonlinear dynamic model based on multibody dynamic methodology to predict contact pressure and sliding distance of metal-on-polyethylene hip prosthesis, simultaneously, under normal walking condition. A closed-form formulation of the contact stresses distributed over the articulating surfaces was derived based upon the elastic foundation model, which reduced computational time and cost significantly. Three-dimensional physiological loading and motions, inertia forces due to hip motion and energy loss during contact were incorporated to obtain contact properties and sliding distance. Comparing the outcomes with that available in the literature and a finite element analysis allowed for the validation of our approach. Contours of contact stresses and accumulated sliding distances at different instants of the walking gait cycle were investigated and discussed. It was shown that the contact point at each instant was located within the zone with the corresponding highest accumulated sliding distance. In addition, the maximum contact pressure and area took place at the stance phase with single support. The stress distribution onto the cup surface also conformed to the contact point trajectory and the physiological loading.

Keywords

---

[1] Corresponding author.

E-mail address: ehsanaskary@gmail.com (E. Askari)

1. Introduction

More than 2 million hip replacements are performed per annum worldwide, which will undergo a twofold increase by 2020 due to an aging population [1]. The 2014 Canadian Joint Replacement Registry also reported that the number of total hip replacements has increased by 16.5% during the last five years [2]. Moreover, the demographics indicate an increase in number of younger patients (45-64 years) and hence, hip arthroplasties are now required to last over 30 years [3], with greater functional demands. Since the early hip implants, the most popular and used combination of hip prostheses has been a metal head on a plastic cup (MoP). This combination suffers from high material loss (wear) of the plastic part with resultant debris leading to osteolysis. The wear is still a key factor in the primary failure of metal-on-polyethylene artificial hip joints, which can influence the performance and life expectancy of an implant [4]. The consequence of wear may be that the patient must undergo revision surgery to replace the original implants with new ones. This is clearly an undesired outcome due to the hardship it imposes on the patient and health budget.

The total hip arthroplasty consists of a femoral stem inserted in the intramedullary canal of the femur and a femoral head fixed to the stem neck, articulating in a cup implanted in the acetabular of pelvis [5]. In a MoP hip prosthesis, the femoral head is made of metal, that is, CoCr and CoCrMo alloy, and stainless steel, while the acetabular cup is ultra-high-molecular-weight polyethylene [5]. The femoral head with a spherical shape slides against the hemispherical cup, restoring the physical functioning of the hip joint as well as reducing pain in most patients [6, 7]. Physiological loading and motions of the hip joint, which alter with time, lead to the movement of the contact point between the cup and femoral head along a trajectory over a gait cycle [8, 9]. Therefore, contact area accommodating contact stresses displaces continuously when patients with implanted hip perform their routine activities. From a mechanical point of view, these physical events in the human body are associated with contact mechanics and dynamics of hip components, among others. Fracture and creep are associated with high contact stresses and it is worth noting that the location of viable fracture and fatigue-related wear can be estimated by knowing where the maximum contact pressure takes place [6, 10-11]. In either designing an optimal patient-specific hip prosthesis or making a clinical decision to properly choose the size and material property of a hip implant for a specific patient, a technical insight of the wear mechanism in hip prostheses in terms of wear distribution and the wear rates are invaluable. Wear of artificial hip joints is influenced by Body-Mass-Index (BMI), activity level, implant size and thickness, clearance, material property, etc. [5, 7, 12]. Focusing on numerical biomechanical modeling, wear prediction requires knowledge of the sliding distance, contact pressure, obtained from dynamic analysis, and tribological data, namely the wear coefficient [4, 13]. Thus, a special attention should be given to the study of contact mechanics and dynamics of hip components.

The shape of slide track is of paramount importance in predicting wear in total hip replacements as any alteration in its shape can lead to a large variation in the resultant

wear rate [14-16]. A theoretical contact point trajectory was presented by Mattei et al. [17] to evaluate wear in which the reaction force between the cup and head was assumed to lay along the direction joining their centers owing to frictionless contact [18]. Another procedure to compute wear was to fix the head center and then tracking the rotations of the femur by imposing physiological rotations [19]. Moreover, Ramamuri et al. [20] selected a number of points on the femoral head and, thereafter, provided their loci of movement during normal gait computationally. Saikko and Calonius [21] developed the Euler rotation method that is computationally promising, and implemented it to calculate slide paths for the so-called three-dimensional motion of the hip joint during walking gait cycle. These procedures calculated contact point path over a gait cycle without taking contact pressure, material properties of colliding bodies and tribological characteristics into account. Therefore, the resultant simplified contact point trajectory does not account for nonlinear characteristics of the relative motion between bearing components, e.g. stick-slip, sliding, impact-contact, friction-induced vibration, damping effect of the plastic cup, etc.

Contact mechanics of metal-on-polyethylene hip prosthesis can be characterized with (1) the Young's modulus of the femoral head is more than 200 times the modulus of the plastic component; (2) the resultant deformations are not small compared to the size of colliding bodies due to low stiffness of the cup; (3) the mating surfaces are conformal [11, 22]. Therefore, physical characteristics of contact in MoP hip arthroplasties seriously violate assumptions made in Hertz contact model. Although it is not applicable to hip implants, Hertz law is frequently applied to the hip joints, particularly for hard-on-hard couplings [6-7]. Several approximated analytical solutions have been proposed to date for soft-on-hard implants, fairly assuming that the ball is rigid compared to the plastic cup. Bartel et al. developed an elasticity model to calculate contact stresses between the cup and the ball, comparing their results to those obtained by the finite element method [11]. Using this elasticity model, Jin and his collaborators conducted a parametric study to explore an optimal design of hip implant to reduce maximum stresses [23]. Tudor et al. developed an elasticity model based on Hill theory and used Erdogan's solution to form a compliance matrix based on which contact stresses can be calculated iteratively [24]. The most widespread approach for solving contact problems is the finite element method (FEM) as it can deal with complex geometries and complex material behaviors and is implemented in commercial codes [10, 25-33]. On the contrary, it involves huge computational time and power.

In addition to artificial hip joints that can be considered as clearance joints, a clearance joint is a common component in much of multibody dynamic mechanisms owing to tolerance and errors in manufacturing and assembly processes as well as wear effect. Radial clearance between joint components leads to impact-contact forces, which reduces reliability and precision and results in noise and vibration. The pioneer compliant (Penalty) method to deal with contact mechanics is Hertzian contact law that also is foundation of most of the available contact force models [34]. Hertzian contact method cannot describe the energy loss during the contact process, while some of the energy is dissipated during the contact-impact process due to friction, plasticity and wave propagation, among others [35]. Hence, other contact force methods have been presented that extend the Hertzian law to accommodate energy dissipation in the form of internal damping [36-43]. However, Hertz contact law and its modified versions are not

appropriate for conformal joint with either very small clearance size or low stiffness component in particular, as discussed for MoP hip joints above. To cope with these difficulties, the elastic foundation model (Winkler model) is widely adopted to determine the contact forces in clearance joints [44-47]. Using Winkler surface model, a numerical iterative scheme is also required to calculate contact forces. In a multibody system analysis, the iteration process has to be handled at each time step over numerical analysis, which is time-consuming and costly.

A few studies predicted both the contact pressure and the sliding distance of artificial knee and hip joints simultaneously. Godest et al. developed an explicit finite element method to estimate the dynamic behavior of the contact mechanics including both the contact mechanics and the kinematics of knee joints, simultaneously [48]. More recently, the method was extended by Gao and his colleagues for a hip implant under normal walking conditions [49]. Askari et al. developed a computational model to investigate both contact point trajectory and contact stresses of ceramic-on-ceramic hip prostheses, simultaneously, using a modified Hertz contact models [9]. Mattei and Di Puccio also proposed a mathematical model in which they employed Hertz contact law to determine both the trajectory and contact pressure distribution in Metal-on-Metal hip implants [50]. The present study thus aimed to develop a nonlinear dynamic model to predict contact pressure and sliding distance of metal-on-polyethylene hip prosthesis, simultaneously, under normal walking condition. A closed-form formulation of contact stresses distributed over the articulating surfaces was derived based on the elastic foundation model, which decreased total computational time significantly compared to available iterative methods. Damping property of the plastic cup was considered in the analysis to account for energy loss during contact and impact scenarios. The developed contact force model as a continuous function of penetration depth took into account information on material and geometric properties of the colliding bodies and damping characteristic of the plastic part. Physiological loading and motions, tribology of articulating bodies and inertia forces due to hip motion were also incorporated into the dynamic analysis. Nonlinear governing motion equations were solved using the adaptive Runge-Kutta-Fehlberg method. A finite element model was also constructed to validate the developed contact model and the dynamic simulation was also verified, compared to those available in the literature. In addition, the accumulated sliding distance and contact pressure at different instants of the walking gait cycle were investigated and discussed. The main contributions of the current research work in multibody dynamics and biomechanics research fields can be highlighted as (*i*) proposing a novel closed-form contact model applicable to conformal clearance joints as common components in multibody dynamic mechanisms; and (*ii*) developing a computational dynamic model to evaluate contact mechanics and sliding distance of soft conformal hip implants, simultaneously.

2. Mathematical modeling

This section focuses on developing mathematical formulations of a hip prosthesis. The hip joint is considered as a clearance joint having six degrees of freedom associated with rotational and translational movement. Although there are no constraints on the dynamic system, it is controlled by contact-impact forces generated owing to contacting the cup

and the femoral head, which is referred to as a force joint because of dealing with force constraints [51]. Physiological loading is applied at the head's center and corresponding motions are assigned to the femoral head, while the plastic cup is considered to be fixed. This arrangement has previously been proposed by Askari et al, introducing a cross section through the center of the femoral head, which was justified mechanically [9, 52]. We consider a head-cup couple of a hip arthroplasty, illustrated in Fig.1, where the femoral head is shown as a sphere for simplicity. P_b and P_c represent possible contact points on the surfaces of the femoral head and cup, respectively. These points locate on the collision plane, which is a plane tangential to the surfaces of femoral head and cup at the contact point. The center of the ball in the global coordinate system is defined by three coordinates (r, Θ, φ) of a spherical coordinate system in which r is the radial distance of the center of the femoral head, O_b, from the cup center, O_c, while φ is the polar angle and Θ is the azimuthal angle. The radial clearance is defined as the difference between the radii of bearing surfaces, $c = R_c - R_b$, where R_c and R_b are the cup and femoral head (ball) radii. Furthermore, the indentation depth of the head inside the cup liner is represented by δ, depicted in Fig. 1. The eccentricity vector, **e**, is also introduced as a vector that connects the point O_c to the point O_b, and the unit vectors, **t** and **n,** represent the tangential and normal directions at the contact point. It is worth noting that the eccentricity vector, **e**, aligns with the normal vector, **n**. In addition to the aforementioned spherical coordinate system, a Cartesian coordinate system is attached at the center of the cup liner, Fig. 1. According to the clinical definitions, the x and z axes point from the lateral to the medial direction (L-M) and from inferior to superior, respectively, while the y axis is parallel to the walking direction, i.e. from posterior to anterior (P-A). The anatomical inclination of the acetabular cup with respect to the horizontal plane is equal to $\pi/4$ as shown in Fig. 1.
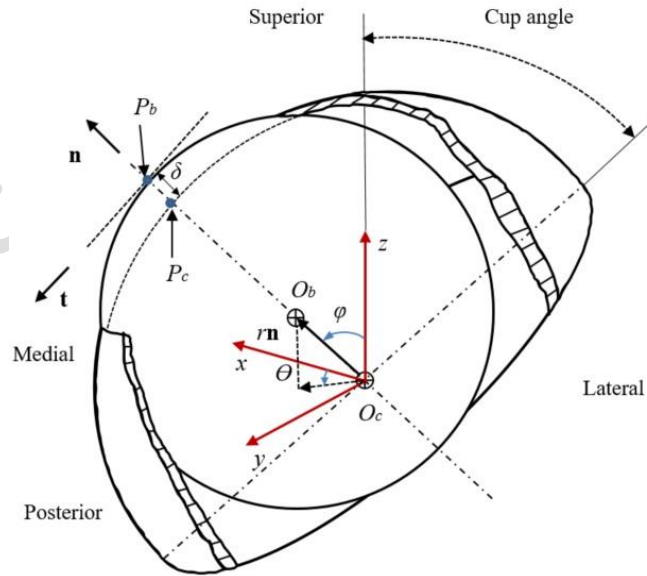
Fig. 1. A schematic representation of the head-cup articulation in which the femoral head is shown as a sphere for the sake of simplicity.

In what follows, the kinematics of the spherical clearance joint are formulated in a vector format for which orthogonal unit vectors in a spherical coordinate system are given by:

$$\mathbf{n} = \mathbf{e}_r = \sin\varphi\cos\theta\mathbf{i} + \sin\varphi\sin\theta\mathbf{j} + \cos\varphi\mathbf{k}$$

$$\mathbf{e}_\theta = -\sin\theta\mathbf{i} + \cos\theta\mathbf{j} + 0\mathbf{k} \tag{1}$$

$$\mathbf{e}_\varphi = \cos\varphi\cos\theta\mathbf{i} + \cos\varphi\sin\theta\mathbf{j} - \sin\varphi\mathbf{k}$$

Evaluating the contact forces needs the calculation of relative normal and tangential velocities of contact points located on both the cup and head surface. Therefore, position vectors of contact points are written as

$$\mathbf{r}_{P_b} = \mathbf{r}_{O_b} + \mathbf{r}_{P_b/O_b} \tag{2}$$

$$\mathbf{r}_{P_c} = \mathbf{r}_{P_c/O_c} \tag{3}$$

where $\mathbf{r}_{P_c/O_c}$ is the vector of the contact point on the cup relative to the cup center, while $\mathbf{r}_{P_c}$ and $\mathbf{r}_{P_b}$ are the position vectors of contact points on the cup and head in the global reference frame with the origin at the cup center, O_c. The relative position vector defined from the contact point on the cup liner to the one on the ball is also given by

$$\mathbf{r}_{P_b/P_c} = \mathbf{r}_{O_b} + \mathbf{r}_{P_b/O_b} - \mathbf{r}_{P_c/O_c} \tag{4}$$

in which

$$\mathbf{r}_{O_b} = r\mathbf{n} \tag{5}$$

that is known as the eccentricity vector. Differentiating Eq. (4) with respect to time results in

$$\mathbf{v}_{P_b/P_c} = \frac{\mathrm{d}}{\mathrm{d}t}\left(\mathbf{r}_{P_b/P_c}\right) = \frac{\mathrm{d}}{\mathrm{d}t}(r\mathbf{n}) + \mathbf{\Omega}_b \times \mathbf{r}_{P_b/O_b} - \mathbf{\Omega}_c \times \mathbf{r}_{P_c/O_c} \tag{6}$$

where

$$\mathbf{\Omega}_b = \omega_x \mathbf{i} + \omega_y \mathbf{j} + \omega_z \mathbf{k} \tag{7}$$

whereas $\mathbf{\Omega}_c$ is zero as the cup is considered to be stationary. Moreover, ω_x, ω_y and ω_z are angular velocities of the ball around the vectors x, y and z, respectively. Consequently, Eq. (6) can be rewritten as

$$\mathbf{v}_{P_b / P_c} = \underbrace{\dot{r}\mathbf{n}}_{v_n \mathbf{n}} + \underbrace{\left(r\dot{\theta}\sin\varphi \mathbf{e}_\theta + r\dot{\varphi}\mathbf{e}_\varphi + \mathbf{\Omega}_b \times R_b \mathbf{n} \right)}_{v_t \mathbf{t}} \tag{8}$$

where

$$\theta = \tan^{-1}(y/x) \tag{9}$$

$$\varphi = \tan^{-1}(\sqrt{x^2 + y^2}/z) \tag{10}$$

$$r = \sqrt{x^2 + y^2 + z^2} \tag{11}$$

$$\dot{\theta} = \frac{\dot{y}x - \dot{x}y}{x^2 + y^2} \tag{12}$$

$$\dot{\varphi} = \frac{zx\dot{x} + zy\dot{y} - \dot{z}x^2 - \dot{z}y^2}{r^2\sqrt{x^2 + y^2}} \tag{13}$$

$$\dot{r} = \frac{x\dot{x} + y\dot{y} + z\dot{z}}{r} \tag{14}$$

Finally, the relative indentation depth is computed, depicted in Fig. 1, by

$$\delta = r - (R_c - R_b) \tag{15}$$

Studying the kinematics of the hip joint, the next subsection will focus on the contact forces.

2.1. Normal contact force models

It is known that modelling normal contact forces has an extremely important contribution in the dynamic behavior of mechanical systems. The contact force model must take into account not only material properties, but geometric characteristics of the contacting bodies. From a computational standpoint, the contact constitutive law should also be stable for the calculation of the contact forces allowing for the integration of the motion equations. As mentioned previously, the elastic half-space theory may not be applicable to the contact problem of total hip arthroplasies because of (1) a much stiffer metal component compared to the plastic one; (2) comparable deformation resulted from physiological loading to the size of bearing parts; and (3) the conformity of mating surfaces. On the other hand, as the displacement at any point in the contact surface depends on the pressure throughout the whole contact, the solution of resultant integral equation based on the elastic contact theory for the pressure causes difficulties to obtain a closed-form contact equation.

This difficulty is simplified in the elastic foundation model where the contact surface is modeled as a set of independent springs scattered over the contact surface [53]. This simplified model does not incorporate deformations at all locations of the bearing generated due to a pressure applied at one location onto the bearing surface, causing the integral nature of contact problems to eliminate. This is contrary to what happens in elastic contact as the displacement at one location is influenced by the pressure applied at other locations. However, the benefits of this simplification can be outlined as (1) faster pressure calculations; (2) facilitated analysis of conformal geometry, nonlinear materials, and layered contact. In what follows, the elastic foundation is discussed in details and later a closed-form contact formulation is derived for MoP hip prostheses.

The springs spread onto the contact surface are considered as linear elastic bars of length h and with a stiffness of E_W. According to the laws of elasticity, the contact pressure for any spring in the elastic foundation is directly related to the spring deformation as

$$P_i = E_W \frac{S_i}{h_i} \tag{16}$$

where P_i is the contact pressure, while E_W represents the elastic modulus for the elastic layer, h_i is the thickness of the elastic layer and S_i is the deformation of the spring, that is, the penetration depth along the normal direction to the undeformed contact surface. When both bodies are deformable, E_W is a composite of the elastic modulus and Poisson's ratio for the two bodies. Readers interested are referred to the references Podra and Andersson [45] and Johnson [47]. In the case of MoP hip implants, it is assumed that only one of the bodies is deformable and a common expression for E_W is given by [54-56]

$$E_W = \frac{(1-\upsilon)E}{(1+\upsilon)(1-2\upsilon)} \tag{17}$$

where E and υ stand for Young's modulus and Poisson's ratio of the elastic layer, respectively. Substituting the notion of E_W in Eq. (16), the following expression is gained for the pressure of any spring

$$P_i = \frac{(1-\upsilon)E}{(1+\upsilon)(1-2\upsilon)}\frac{S_i}{h_i} \tag{18}$$

Having the pressure distribution function at hand, the total normal contact force can be computed by integrating the resultant load due to the pressure at each element over the contact area, Fig. 2. To facilitate this process, the contact area and penetration depth are specified as functions of the contact angle, ψ. Assuming the femoral head penetrates the cup surface as can be seen in Fig. 2, the spherical head and hemisphere socket intersect along a circle forming the circumference of the contact area. The contact radius can be determined intersecting two circle equations, Eq. 19a, b, of the cup and the femoral head in any two-dimensional cross section crossing the centers of hip components.

$$r_1 = R_c, \tag{19a, b}$$
$$r_2^2 - 2r_2 e\cos(\psi) + e^2 = R_b^2$$

where e is the size of the eccentricity vector and ψ is specified in Fig. 2. Moreover, r_1 and r_2 represent the radial distance of any point of the circles associated with the cup and femoral head, respectively, in the global coordinate system with the origin at O_c, Fig. 2.
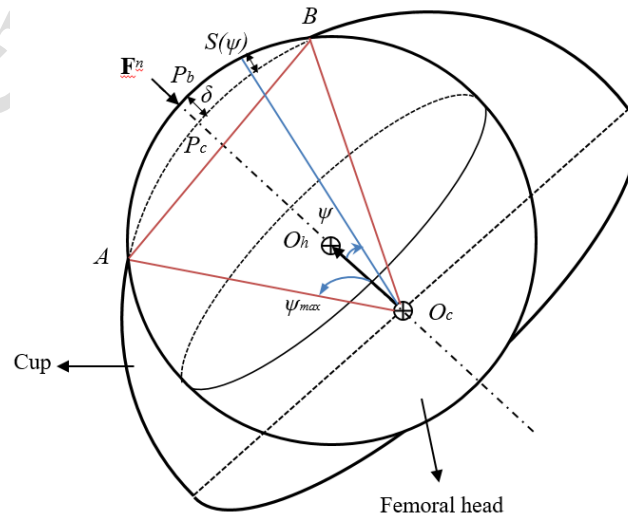

Fig. 2. A schematic representation of contact area and penetration depth.

(A) and (B) shown in Fig 2 are points at which circles defined by Eq. (19a, b) intersect, which can be determined by substituting r_2 with R_c that results in the following expression

$$\cos(\psi_{max}) = \frac{R_c^2 - R_b^2 + e^2}{2R_c e} \tag{20}$$

and the contact radius is thus gives by:

$$\frac{\overline{AB}}{2} = \sqrt{R_c^2 - \left(\frac{R_c^2 - R_b^2 + e^2}{2e}\right)^2} \tag{21}$$

Solving the quadratic equation for r_2, 19b, the radial penetration of spring elements within the contact area can be calculated simply by the expression of $(r_2 - r_1)$, so

$$S(\psi) = (r_2 - r_1) = e\cos(\psi) + R_b\sqrt{1 - \left(\frac{e}{R_b}\right)^2 \sin(\psi)^2} - R_c \tag{22}$$

and the total normal contact force, f_n, can be computed from the following integration:

$$f_n = \iint_{\Xi} P dA \tag{23}$$

where Ξ is the contact area, dA can be written as $2\pi R_c^2 \sin(\psi)\cos(\psi)d\psi$ and pressure function as $\frac{E_W}{h}S(\psi)$. The integration can therefore be performed over the interval [0, ψ_{max}]

$$f_n = 2\pi \int_0^{\psi_{max}} \frac{E_W}{h} S(\psi) R_c^2 \sin(\psi)\cos(\psi)d\psi \tag{24}$$

After some mathematical manipulation, the total normal contact force can finally be expressed as

$$f_n = \frac{2\pi K}{h} R_c^2 \left[\frac{e}{3}(1 - \cos(\psi_{max})^3) \right.$$

$$+ \frac{R_b}{3}\left(\frac{R_b}{e}\right)^2 \left\{ 1 - \left(1 - \left(\frac{e}{R_b}\right)^2 \sin(\psi_{max})^2 \right)^{3/2} \right\}$$

$$\left. - \frac{R_c}{2}(1 - \cos(\psi_{max})^2) \right] \qquad (25)$$

The contact force vector between the femoral head and cup is, therefore, governed by

$$\mathbf{F}_{p_b}^n = f_n \mathbf{n} \equiv H(\delta)\mathbf{n} \qquad (26)$$

where f_n is a function of δ which is the maximum relative penetration depth given by Eq. (15). Additionally, the superscript n stands for the normal direction to the collision plane and the subscript P_b represents the contact point on the femoral head. This law, however, cannot capture the energy loss due to contact-impact events. In the Kelvin-Voigt model, the energy loss was taken into account by a linear damping term [57]. The contact force model can therefore, be written in terms of a damping coefficient D as $f_n = H(\delta) + D\dot{\delta}$. Moreover, Hunt and Grossley suggested a hysteresis form for the damping coefficient as $D = \acute{\chi}H(\delta)$ [37]. Thus, the normal contact load can be given by [58],

$$f_n \equiv f_n(\dot{\delta}, \delta) = H(\delta)$$

$$+ \acute{\chi}H(\delta)\dot{\delta} \qquad (27)$$

where $\dot{\delta}$ is the relative penetration velocity of the contact and $\acute{\chi}$ denotes the hysteresis damping factor for which a number of available models are listed in Table 1 . $\dot{\delta}^{(-)}$ denotes the initial impact velocity and c_e represents the coefficient of restitution [59].

Table 1. Models of the hysteresis damping factor regarding Eq. (27)

Viscous damping model	Governing law for $\acute{\chi}$
Hunt and Crossley [37], Marefka and Orin [60]	$\dfrac{3(1 - c_e)}{2}\dfrac{1}{\dot{\delta}^{(-)}}$
Herbert and McWhannell [61]	$\dfrac{6(1 - c_e)}{[(2c_e - 1)^2 + 3]}\dfrac{1}{\dot{\delta}^{(-)}}$
Lee and Wang [62]	$\dfrac{3(1 - c_e)}{4}\dfrac{1}{\dot{\delta}^{(-)}}$
Lankarani and Nikravesh [39]	$\dfrac{3(1 - c_e{}^2)}{4}\dfrac{1}{\dot{\delta}^{(-)}}$

Gonthier et al. [63] Zhang and Sharf [64]	$\dfrac{(1-c_e{}^2)}{c_e}\dfrac{1}{\dot\delta^{(-)}}$
Zhiying and Qishao [65]	$\dfrac{3(1-c_e{}^2)e^{2(1-c_e)}}{4}\dfrac{1}{\dot\delta^{(-)}}$
Flores et al. [43]	$\dfrac{8(1-c_e)}{5c_e}\dfrac{1}{\dot\delta^{(-)}}$
Gharib and Hurmuzlu [66]	$\dfrac{1}{c_e}\dfrac{1}{\dot\delta^{(-)}}$

2.2. Dynamic governing equations of the system

In this section, the free body diagram of the hip ball is drawn, illustrated in Fig. 3, and the corresponding equations of motion are subsequently derived. The femoral head rotates around the x, y and z axes, representing flexion-extension (FE), abduction-adduction (AA) and internal-external rotation (IER) respectively. The contact forces are evaluated according to the governing equations presented above and then transferred to the center of the femoral head. The equations of motion are therefore obtained using Newton's Second law, as follows :

$$\sum F_X = m\ddot{x}, \qquad \sum F_X = f_x + \left(\mathbf{F}_{p_b}^t + \mathbf{F}_{p_b}^n\right)\cdot\mathbf{i}\langle\delta\rangle^0$$

$$\sum F_Y = m\ddot{y}, \qquad \sum F_Y = f_y + \left(\mathbf{F}_{p_b}^t + \mathbf{F}_{p_b}^n\right)\cdot\mathbf{j}\langle\delta\rangle^0 \tag{28}$$

$$\sum F_Z = m\ddot{z}, \qquad \sum F_Z = f_z + \left(\mathbf{F}_{p_b}^t + \mathbf{F}_{p_b}^n\right)\cdot\mathbf{k}\langle\delta\rangle^0 - mg$$
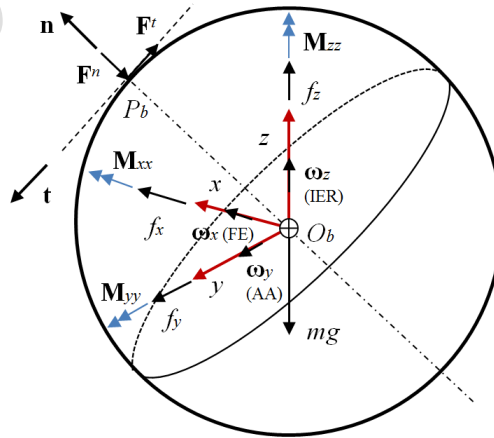

Fig. 3. Free body diagram of the ball (the femoral head).

in which $\langle\ \rangle^0$ is Heaviside function, this is

$$\langle\delta\rangle^0 = \begin{cases} 1 & \delta > 0 \\ 0 & \delta \leq 0 \end{cases} \tag{29}$$

where $\delta > 0$ identifies when the hip components are in contact and $\delta \leq 0$ for free-flight mode. The contact forces are effective provided that the contact mode is on [66]. Furthermore, the rebound and impact velocities and location should be acquired as initial conditions in order for solving motion equations of following dynamic scenario that are either contact mode or free flight. In addition to velocities, time at which either impact or rebound occurs plays a critical role, which can be detected by satisfying the following condition during the numerical solution by progressing time:

$$\delta(t^i) < 0, \quad \delta(t^{i+1}) > 0 \tag{30}$$

The equations of motion can finally be written as

$$\begin{bmatrix} m & 0 & 0 \\ 0 & m & 0 \\ 0 & 0 & m \end{bmatrix}\begin{bmatrix} \ddot{x} \\ \ddot{y} \\ \ddot{z} \end{bmatrix} = \begin{bmatrix} f_x + \left(\mathbf{F}_{p_b}^t + \mathbf{F}_{p_b}^n\right)\cdot\mathbf{i}\langle\delta\rangle^0 \\ f_y + \left(\mathbf{F}_{p_b}^t + \mathbf{F}_{p_b}^n\right)\cdot\mathbf{j}\langle\delta\rangle^0 \\ f_z + \left(\mathbf{F}_{p_b}^t + \mathbf{F}_{p_b}^n\right)\cdot\mathbf{k}\langle\delta\rangle^0 - mg \end{bmatrix} \tag{31}$$

The resulting equations, Eq. (31), are nonlinear and can be solved utilizing a numerical method. In this study, the adaptive Runge-Kutta-Fehlberg method is employed to integrate Eq. (31) in time [67].

2.3. Validation

In this study, a MoP artificial hip joint with the following characteristics was considered. The metallic component was represented with the following material properties: 210 GPa Young's modulus, 0.3 Poisson's ratio and 8330 kg/m3 density, while the polyethylene cup was characterized with Young's modulus of 0.5 GPa and 0.4 as Poisson's ratio. The hip implant is modelled as a joint with a clearance size of 80 μm and restitution coefficient 0.7, while the effect of friction on the dynamics of hip prosthesis was neglected. Moreover, the internal radius of the acetabular cup was assumed to be 14 mm, while the femoral head had a 13.92 mm radius. Two analyses were subsequently performed (1) to compare the contact model against a FE model and (2) to study nonlinear dynamics and contact mechanics of the hip prosthesis.

The contact methodology developed based on the elastic foundation model was verified against a finite element analysis. A three-dimensional configuration of the hip implants was utilized using the commercial software ANSYS workbench (Release 17.1). The outer surface of the acetabular cup was fixed as it was considered that the cup was fully bonded to the metal backing. The type of analysis was set as static to evaluate contact pressure and contact radius and a frictionless contact was defined between bearing surfaces. Four magnitudes of the vertical load, f_z, within the range of in vivo loading reported by Bergman et al. were chosen, based on which the FE analyses were performed [69]. Moreover, the FE analyses were performed for multiple clearance sizes, hip sizes, liner thicknesses and material properties while a fixed vertical load, 500 N, was considered. Contact elements were sized small enough to guarantee the convergence and accuracy of results, performing a mesh sensitivity analysis, refining contact elements in particular, and employing a fine smoothing scheme, Fig. 4. The numbers of element and node used for the present FE modeling were 73073 and 119981, respectively.

Moreover, the governing motion equations of a MoP artificial hip joint with clearance were solved for the dynamic simulation of the hip arthroplasty as described in the preceding lines. Viscous damping model proposed by Gonthier at al. and Zhang and Sharf was used in the present study as this model also accounts for soft material contact with medium value of the coefficient of restitution. Three-dimensional physiological forces and angular motions were sourced from the literature and shown in Figs. 5 and 6 [69]. Initial joint anlges were also set regarding data available in Fig. 5. The dynamic response of the system was obtained by solving the equations of motion using the adaptive Runge-Kutta-Fehlberg method. To acquire accurate and stable outcomes, an error threshold was defined. At each time step of dynamic simulation, the error magnitude was assessed by comparing results obtained from the explicit method with different orders. When the error magnitude was greater than the error threshold, the time step is halved and computation re-done. In this process, the minimum value for the integration step size was considered to be 100 ns and the corresponding integration tolerance 10. Moreover, the cup surface was discretized into several elements and the accuracy and convergence study were performed to evaluate the mesh density in order for the representation of contact stress distribution and accumulated sliding distance. Consequently, the number of elements was chosen 8100 on the cup surface. The computational method was stable and solutions to the equations always achieved. In the next section, the results of solutions for Eq. (31) for artificial hip joints will be presented and discussed.
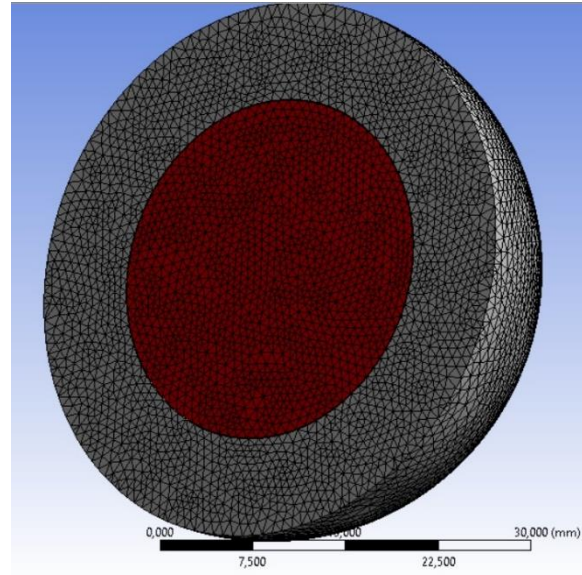
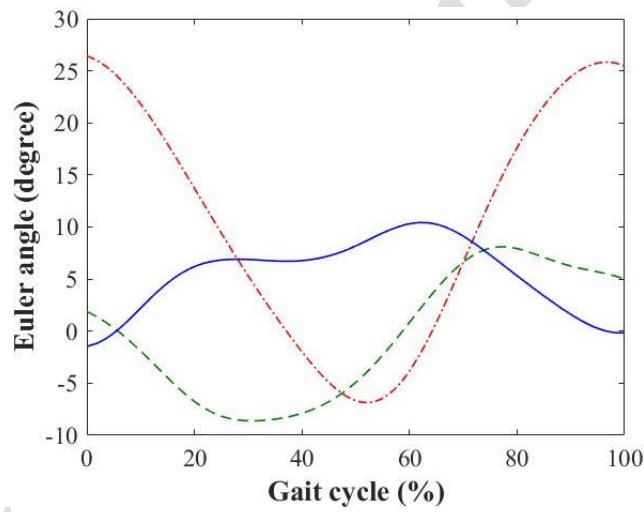Fig. 4. A representation of meshed femoral head (in red) inside the cup surface

Fig. 5. The Euler angles due to the physiological motion of the femoral head where γ (internal-external rotation (IER)); β (abduction-adduction (AA)); α (flexion-extension (FE)).
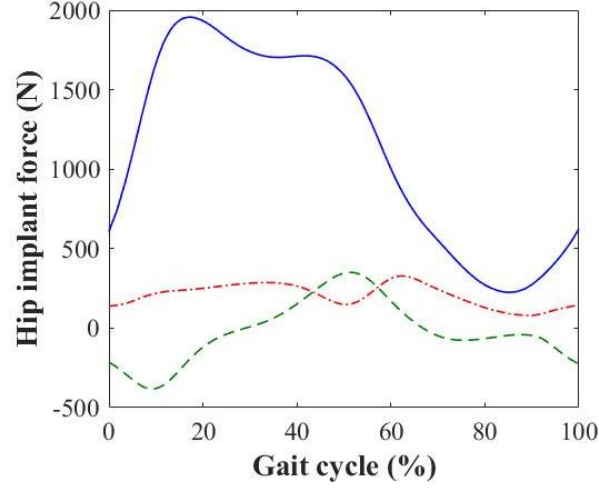
Fig. 6. Physiological adopted forces with f_z (Vertical); f_y (A-P); f_x (M-L) for the gait cycle.

3. Results and discussion

The maximum contact pressures and contact radii acquired from both FEA and the developed dynamic model are listed in Tables 2 and 3. A good agreement was found between outcomes obtained from two methods with discrepancies within 7.11 percent with respect to those from FEA. Moreover, Tables 2 and 3 listed contact pressures and contact radii obtained from Hertz contact model. It can be seen that Hertzian contact model was not suitable for the soft conformal contact in hip implants as the maximum error was found out to be more than 34%. Table 2 presented results associated with multiple loadings while Table 3 studied and compared outcomes acquired from the developed model with those from FE analyses and Hertz contact law for three different clearance sizes, hip sizes, liner thicknesses and material properties. Hertz contact law did not capture the variation in liner thickness while the developed model complied with the FE model. Fig. 7 shows contact pressure distribution within the contact interface between the femoral head and cup with an applied load of 1500 N. It is worth highlighting that the contact model developed by the current study was based on the elastic foundation method, but the model derived was similar to the elasticity solution of Bartel et al. except of the stiffness coefficient, E_W/h, Eqs. (17) and (18), [11]. However, a comparison between those coefficients in the current model and Bartel et al's for all cases considered in the present work showed a deviation less than 3%. Maximum contact stresses obtained from the developed methodology were less than those from FEA, while an opposite trend can be observed for contact radii. This outcome conformed to the reference [11]. In addition to developing a contact model based on the elastic foundation method, the current study proposed a closed-form contact formulation for conformal contact in metal-on-polyethylene hip arthroplasties. Hertz contact law is not applicable for conformal contact in MoP hip implants and commonly FEM is employed to determine contact characteristics. On the other hand, FEM is not relatively efficient in terms of

computational time and cost, especially for performing parametric studies for optimizing and assessing implant new designs. Moreover, one of main goals to decrease computational time and create independent software tool is to help doctors make an optimal decision for patient-specific implants as fast and accurate as possible. Such a decision can be made taking into account patient factors and parameters such as physiological loadings/motions associated with different daily activities, activity level, age, gender and so forth. Considering a FE code that can be run independently without any support of a commercial software to reduce costs involved, the FE modeling would still be a time consuming option in order to consider multiple loadings and motion scenarios. The closed-form contact model developed in the present paper showed a relatively good accuracy compared to FE results. Moreover, total computation time for the present method was no longer than 20 minutes, whereas Gao et al. reported a total computational time of about 4 and 5 hours for implicit and explicit finite element simulations, respectively, [49, 69]. It is worth noting that the presented model is unable to address accurate contact pressure and contact area once the edge-loading occurs due to its simplification of the model that limits it to capture the geometry change at the cup edge. FE method, therefore, should be employed to analyze the edge-loading phenomenon.

Table 2. A comparison between results obtained from both FEM and the developed model.

Applied force (N)	Pmax (MPa)			Contact radius (mm)		
	FEM	Developed model	Hertz model	FEM	Developed model	Hertz model
250	2.41	2.47	2.3	7.45	7.98	7.27
500	3.57	3.57	2.8	8.62	9.20	9.16
1000	5.47	5.46	3.6	9.94	10.50	11.54
1500	7.14	7.10	4.1	10.6	11.20	13.22
2000	8.65	8.56	4.5	11.04	11.6	14.55

Table 3. A comparison between results obtained from both FEM and the developed model: considering clearance size, hip size, liner thickness and material property

Applied force (N)		Pmax (MPa)			Contact radius (mm)		
		FEM	Developed model	Hertz model	FEM	Developed model	Hertz model
Clearance (μm)	80	3.57	3.57	2.8	8.6	9.2	9.2
	100	3.94	4.01	3.3	8.2	8.7	8.5
	200	5.28	5.45	5.3	7.3	7.4	6.7
Hip size (mm)	14	3.57	3.57	2.8	8.6	9.2	9.2
	16	2.93	2.9	2.4	9.3	9.7	10.0
	18	2.55	2.63	2	10.38	10.5	10.8
	8	3.57	3.57	2.8	8.6	9.2	9.2

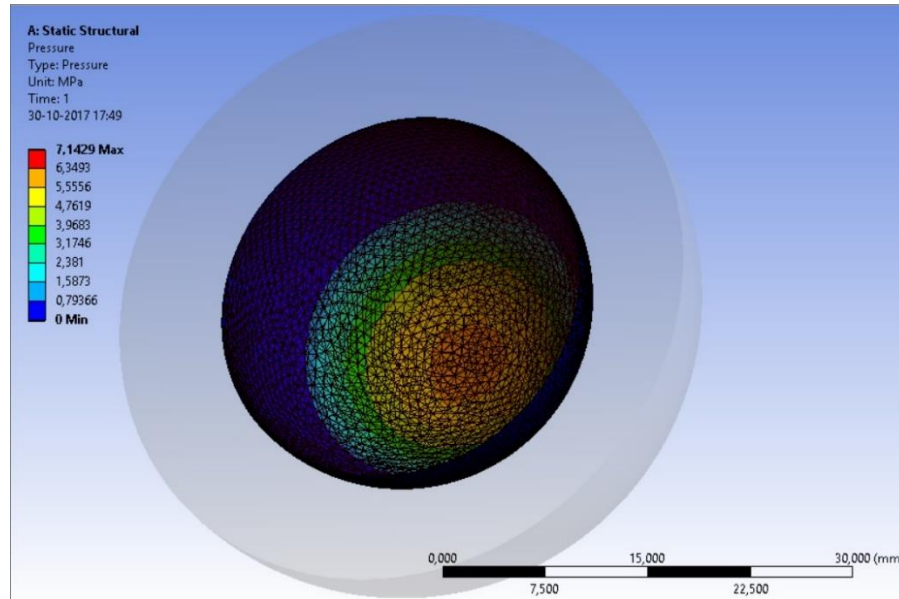|							
cup thickness (mm)	12	3.25	3.28	2.8	9.1	9.3	9.2
	16	3.06	2.95	2.8	9.2	9.5	9.2
Young's modulus (GPa)	0.5	3.57	3.57	2.8	8.6	9.2	9.2
	1	4.81	4.78	4.5	7.5	8.0	7.3
	2	6.59	6.49	7.1	6.5	6.9	5.8

Fig. 7. Contact pressure distribution due to the femoral head and cup contact. The load normally applied on the hemisphere sphere of the cup is 1500 N. The maximum pressure is 7.14 MPa.

The contact stresses and contact area between the femoral head and cup of artificial hip joints are key determinants of implant wear. The maximum contact pressure was illustrated in Fig. 8 as a function of time. The maximum value took place at the stance phase with single support where the resultant physiological force is just less than 2 kN. Contact pressure distributed onto the cup surface due to three-dimensional physiological loading and multidirectional motions at different walking instants were also represented in Fig. 9. On top of pressure contours, the corresponding contact point and path can also be observed which helped comprehend stress distribution more in details. In this set of results, the maximum pressure occurred at 20 percentage of the gait where the contact also possessed the biggest radius. The minimum stress and contact radius belonged to the plot at which 80% of the gait was reached. These pressure contours conformed the physiological loading and the contact point path.
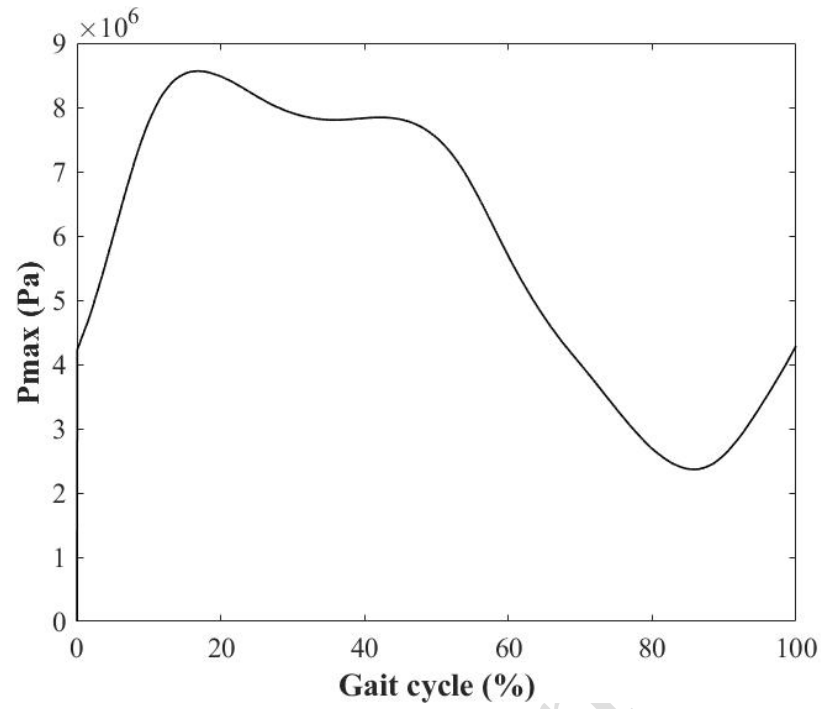
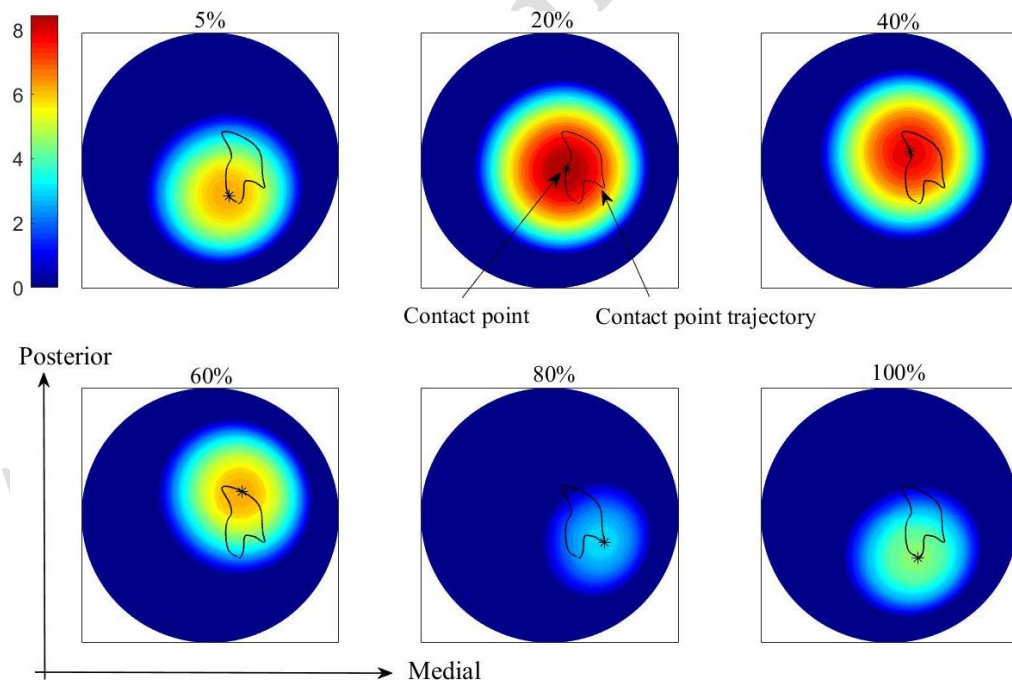Fig. 8. Maximum contact pressure of a hip implant with respect to time.

Fig. 9. Contours of the contact pressure (MPa) at different percentage of the gait cycle for the artificial hip joint.

The sliding distance has a significant influence on the computed wear rates as observed in Archard's wear methodology [14]. Owing to the crucial significance of slide track and wear, this section aims to dynamically study the magnitude and distribution of the sliding distance with time during a gait cycle. Fig. 10 represented the sliding distance as a function of time, while compared to that obtained from the Euler rotation method proposed by Saikko and Calonius [21]. The Euler rotation method does not incorporate contact mechanics, tribology of bearing surfaces and inertia forces due to components motion. Therefore, the goal of the present study was to dynamically investigate the sliding distance and slide track simultaneously. This dynamic model specified those points onto the cup surface that were located within the contact area and calculated both sliding distance and contact pressure related to each point. Although a good agreement between results obtained from these two models can be observed, a greater amount of sliding distance was acquired by the developed model at the end of the gait cycle. The total value is 23.1 mm vs 21.0 mm obtained by Saikko and Calonius's approach [21]. Kang et al reported an overall sliding distance of 23.38 mm, while it was calculated 20.31 mm by Gao et al. using a finite element analysis [49, 70].
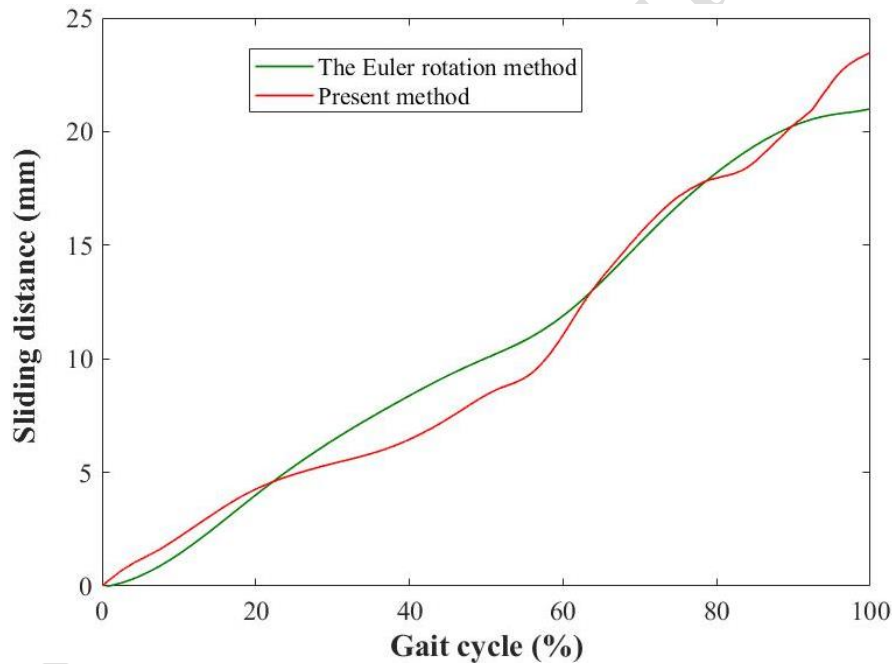

Fig. 10. Comparison of computed sliding distance with that reported by Calonius and Saikko [21].
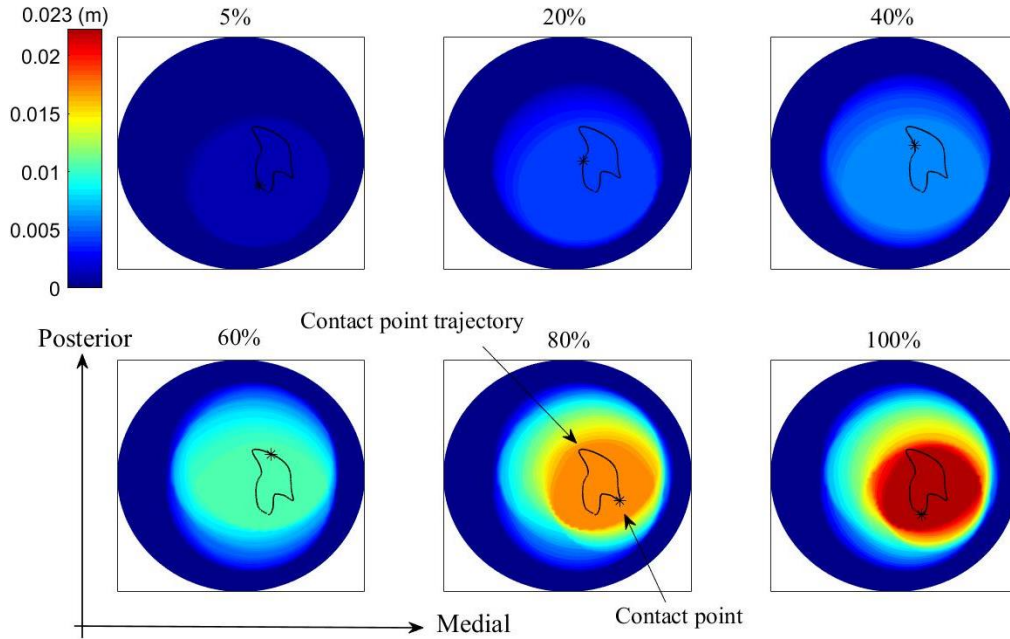
Fig. 11. Contours of the cup inner accumulated sliding distance (m) at difference percentage of the gait cycle for the conventional artificial hip joint model predicted by the present model

The current model allowed exploring the accumulation of sliding distance at each point onto the cup surface at each instant of the walking gait cycle, depicted in Fig. 11. The contact point trajectory and contact point were also illustrated and it can be seen that the accumulated sliding distance gradually increased until the end of the gait at which a maximum value of 23.1 was reached. It can be concluded that the contact point at each instant was located within the zone with the corresponding highest accumulated sliding distance. As can be seen, the contours conformed to the corresponding trajectories of contact point in terms of location and shape. The dark red color in the last map illustrated the area where the maximum sliding distance took place. The linear wear rate is directly associated with the contact pressure and sliding distance regarding Archard wear law. It can therefore be concluded that the maximum linear wear rates took place where those parameters took higher values.

4. Conclusion

Initially, drawbacks involved in employing the finite element method and Hertz contact law were understood and a closed-form contact formulation based on the elastic foundation method was developed for metal-on-polyethylene hip arthroplasties. This model reduced computational time associated with identifying contact characteristics

compared to available iterative methods. The model was subsequently integrated into a nonlinear dynamic formulation to predict contact pressure and sliding distance of metal-on-polyethylene hip prosthesis, simultaneously, under normal walking condition, reducing computational time and cost significantly. The approach incorporated tribology of bearing surfaces, inertia forces due to hip motion, three-dimensional physiological loading and motions and damping property of the plastic cup. The model showed a good accuracy, compared to that available in the literature and a finite element analysis. Moreover, it was observed that the total computational time required for this approach was no longer than 20 minutes, although 4 and 5 hours were required for implicit and explicit finite element simulations, reported by previous studies. The resulting contact pressure distribution and accumulated sliding distance at multiple instants of the walking gait cycle were obtained and discussed, conforming to previous research studies available in the literature. Finally, the presented model is a general methodology being also applicable to multibody systems with conformal clearance joints, e.g. revolute joints.

Acknowledgment

Conflicts of interest

Authors have none to declare.

References

[1] S. Kurtz, K. Ong, E. Lau, F. Mowat, Halpern M., Projections of primary and revision hip and knee arthroplasty in the United States from 2005 to 2030. The Journal of Bone & Joint Surgery, 89(4) (2007) 780-785.

[2] Canadian Joint Replacement Registry 2014 Annual Report. Canadian institute for health information. Canada2014.

[3] NJR 10th Annual Report 2013, National Joint Registry UK 2013.

[4] I.C. Clarke, V. Good, P. Williams, D. Schroeder, L. Anissian, A. Stark, H. Oonishi, J. Schuldies, G. Gustafson, Ultra-Low Wear Rates for Rigid-on-Rigid Bearings in Total Hip Replacements. Proceedings of the Institution of Mechanical Engineers, Part H: Journal of Engineering in Medicine, 214(4) (2000) 331-47.

[5] E. Askari, P. Flores, D. Dabirrahmani, R. Appleyard, A review of squeaking in ceramic total hip prostheses. Tribology International 93 (2016) 239–256.

[6] E. Askari, P. Flores, D. Dabirrahmani, R. Appleyard, Dynamic modeling and analysis of wear in spatial hard-on-hard couple hip replacements using multibody systems methodologies. Nonlinear Dynamics 76 (2014) 1365-1377.

[7] L. Mattei, F. Di Puccio, B. Piccigallo, E. Ciulli, Lubrication and wear modelling of artificial hip joints: a review. Tribology International 44(5) (2011) 532-549.

[8] B. Ramamurti, C.R. Bragdon, D.O. O'Connor, J.D. Lowenstein, M. Jasty, D.M. Estok, W.H. Harris, Loci of movement of selected points on the femoral head during normal gait: three-dimensional computer simulation. J. Arthroplast. 11(7) (1996) 845-852

[9] E. Askari, P. Flores, D. Dabirrahmani, R. Appleyard, Nonlinear vibration and dynamics of ceramic on ceramic arti- ficial hip joints: a spatial multibody modelling. Nonlinear Dyn. 76 (2014) 1365-1377

[10] Z.M. Jin, S.M. Heng, H.W. Ng, D.D. Auger, An axisymmetric contact model of ultra high molecular weight polyethylene cups against metallic femoral heads for artificial hip joint replacements. Proc Inst Mech Eng H. 213(4) (1999) 317-27.

[11] D.L. Bartel, A.H. Burstein, M.D. Toda, D.L. Edwards, The effect of conformity and plastic thickness on contact stress in metal-backed plastic implants. Trans. ASME, J. Biomech. Engng 107 (1985) 193-199.

[12] W.L. Walter, S.M. Kurtz, C. Esposito, W. Hozack, K.G. Holley, J.P. Garino, M.A. Tuke, Retrieval analysis of squeaking alumina ceramic-on-ceramic bearings. J. Bone Joint Surg. 93-B(2) (2011) 1597-1601

[13] V. Hegadekatte, N. Huber, O. Kraft, Finite element based simulation of dry sliding wear. Modelling and Simulation in Materials Science and Engineering, 13 (2005) 57-75.

[14] J.F. Archard, Contact and rubbing of flat surfaces. J. Appl. Phys. 24 (1953) 981-988.

[15] P.S.M. Barbour, M.H. Stone, J. Fisher, A hip joint simulator study using simplified loading and motion cycles generating physiological wear paths and rates. Proc. Inst. Mech. Eng. Part H 213(6) (1999) 455-467

[16] V. Saikko, O. Calonius, J. Kernen, Effect of slide track shape on the wear of ultra-high molecular weight polyethylene in a pin-on-disk wear simulation of total hip prosthesis. J. Biomed. Mater. Res. Part B 69 B(2) (2004) 141-148

[17] L. Mattei, F. Di Puccio, E. Ciulli, A comparative study of wear laws for soft-on-hard hip implants using a mathematical wear model. Tribol. Int. 63 (2013) 66-77

[18] M.T. Raimondi, C. Santambrogio, R. Pietrabissa, F. Raffelini, L. Molfetta, Improved mathematical model of the wear of the cup articular surface in hip joint prostheses and comparison with retrieved components. Proc. Inst. Mech. Eng. Part H 215(4) (2001) 377-391

[19] F. Jourdan, A. Samida, An implicit numerical method for wear modeling applied to a hip joint prosthesis problem. Comput. Methods Appl. Mech. Eng. 198 (2009) 2209–2217

[20] B. Ramamurti, C.R. Bragdon, D.O. O'Connor, J.D. Lowenstein, M. Jasty, D.M. Estok, W.H. Harris, Loci of movement of selected points on the femoral head during normal gait: three-dimensional computer simulation. J. Arthroplast. 11(7) (1996) 845–852

[21] V. Saikko, O. Calonius, Slide track analysis of the relative motion between femoral head and acetabular cup in walking and hip simulator. J. Biomech. 35(4) (2002) 455-464

[22] F. Di Puccio, L. Mattei, Biotribology of artificial hip joints. World J Orthop 6(1) (2015) 77-94.

[23] Z.M. Jin, D. Dowson, J. Fisher, A parametric analysis of the contact stress in ultra-high molecular weight poly ethylene acetabular cups. Med. Engng Phys. 16(5) (1994) 398–405.

[24] A. Tudor, T. Laurian, V.M. Popescu, The effect of clearance and wear on the contact pressure of metal on polyethylene hip prostheses. Tribology International 63 (2013) 158–168.

[25] T. Maxian, T. Brown, D. Pedersen, J. Callaghan, 3-Dimensional sliding-contact computational simulation of total hip wear. Clinical Orthopaedics and Related Research 333 (1996) 41–50.

[26] T.D. Brown, K.J. Stewart, J.C. Nieman, D.R. Pedersen J.J. Callaghan, Local head roughening as a factor contributing to variability of total hip wear: a finite element analysis. Journal of Biomechanical Engineering 124(6) (2002) 691–8.

[27] P.S.M Barbour, R.C. Barton, N. Fisher, The influence of contact stress on the wear of UHMWPE for total replacement hip prostheses. Wear 181-183 (1995) 250–257.

[28] A. Wang, A. Essner, R. Klein, Effect of contact stress on friction and wear of ultra-high molecular weight polyethylene in total hip replacement. Proceedings of the Institution of Mechanical Engineers, Part H (Journal of Engineering in Medicine) 215(H2) (2001)133–9.

[29] L. Kang, A.L. Galvin, J. Fisher, Z.M. Jin, Enhanced computational prediction of polyethylene wear in hip joints by incorporating cross-shear and contact pressure in additional to load and sliding distance: effect of head diameter. Journal of Biomechanics 42(7) (2009) 912–8.

[30] F.C. Wang, Microscopic asperity contact and deformation of ultrahigh molecular weight polyethylene bearing surfaces. Proceedings of the Institution of Mechanical Engineers, Part H: Journal of Engineering in Medicine 217(6) (2003) 477–490.

[31] G. Matsoukas, R. Willing, Y. Kim, Total Hip Wear Assessment: A Comparison Between Computational and In Vitro Wear Assessment Techniques Using ISO 14242 Loading and Kinematics. J Biomech Eng 131(4),

[32] F. Liu, A. Galvin, Z.M. Jin, J. Fisher, A new formulation for the prediction of polyethylene wear in artificial hip joints. Proceedings of the Institution of Mechanical Engineers, Part H: Journal of Engineering in Medicine 225(1) (2011) 16-24.

[33] X. Hua, J. Li, L. Wang, Z. Jin, R. Wilcox, J. Fisher, Contact mechanics of modular metal-on-polyethylene total hip replacement under adverse edge loading conditions. Journal of Biomechanics 47 (2014) 3303-3309.

[34] H. Hertz, Über die Berührung fester elastischer Körper. J. reine angewandte Mathematik 92 (1881) 156-171.

[35] W.J. Stronge, Impact Mechanics, Cambridge: Cambridge University Press, 2000.

[36] M. Machado, P. Moreira, P. Flores, et al.: Compliant contact force models in multibody dynamics: evolution of the Hertz contact theory. Mech. Mach. Theory 53 (2012) 99-121.

[37] K.H. Hunt, F.R.E. Crossley, Coefficient of restitution interpreted as damping in vibroimpact, J. Appl. Mech. 7 (1975) 440-445.

[38] H.M. Lankarani, P.E. Nikravesh, A contact force model with hysteresis damping for impact analysis of multibody systems, J. Mech. Des. 112 (1990) 369-376.

[39] H.M. Lankarani, P.E. Nikravesh, Continuous contact force models for impact analysis in multibody systems. Nonlinear Dyn. 5(2) (1994) 193-207.

[40] Z. Bai, Y. Zhao, A hybrid contact force model of revolute joint with clearance for planar mechanical systems. Int. J. Non Linear Mech. 48(48) (2013) 15-36.

[41] O. Muvengei, J. Kihiu, B. Ikua, Dynamic analysis of planar rigid-body mechanical systems with two-clearance revolute joints. Nonlinear Dyn. 73(1–2) (2013) 259-273.

[42] X. Zhang, X. Zhang, Z. Chen, Dynamic analysis of a 3-RRR parallel mechanism with multiple clearance joints. Mech. Mach. Theory 78(78) (2014) 105–115.

[43] P. Flores, M. Machado, M.T. Silva, J.M. Martins, On the continuous contact force models for softmaterials inmultibody dynamics, Multibody Syst. Dyn. 25 (2011) 357–375.

[44] A. Flodin, S. Andersson, Simulation of mild wear in spur gears. Wear 207(1-2) (1997) 16-23.

[45] P. Põdra, S. Andersson, Wear Simulation With the Winkler Surface Model. Wear, 207 (1997) 79–85.

[46] C.S. Liu, K. Zhang, R. Yang, The FEM analysis and approximate model for cylindrical joints with clearances. Mech. Mach. Theory 42(2) (2007) 183–197.

[47] K.L. Johnson, Contact Mechanics, Cambridge University Press, Cambridge, 1985.

[48] A.C. Godest, M. Beaugonin, E. Haug, et al. Simulation of a knee joint replacement during a gait cycle using explicit finite element analysis. J Biomech 35 (2002) 267-275.

[49] Y. Gao, Z. Jin, L. Wang, M. Wang, Finite element analysis of sliding distance and contact mechanics of hip implant under dynamic walking conditions. Proc IMechE Part H: J Engineering in Medicine 229(6) (2015) 469–474.

[50] L. Mattei, F. Di Puccio, Wear simulation of metal-on-metal hip replacements with frictional contact. J. Tribol. 135(2) (2013).

[51] P. Flores, H.M. Lankarani, Spatial rigid-multi-body systems with lubricated spherical clearance joints: modeling and simulation. Nonlinear Dyn. 60 (2010) 99–114

[52] E. Askari, P. Flores, D. Dabirrahmani, R. Appleyard, Study of the friction-induced vibration and contact mechanics of artificial hip joints. Tribol. Int. 70 (2014) 1–10

[53] S. Mukras, N.H. Kim, A. Nathan, Mauntler, Tony Schmitz, W. Gregory Sawyer. Comparison Between Elastic Foundation and Contact Force Models in Wear Analysis of Planar Multibody System. Journal of Tribology132 (3) (2010).

[54] G. Li, M. Sakamoto, E.Y.S. Chao, A Comparison of Different Methods in Predicting Static Pressure Distribution in Articulating Joints. J. Biomech., 30 (1997) 635–638.

[55] Y. Bei, B.J. Fregly, Multibody Dynamic Simulation of Knee Contact Mechanics, Med. Eng. Phys., 26 (2004) 777–789.

[56] K.N. An, S. Himenso, H. Tsumura, T. Kawai, E.Y.S. Chao, Pressure distribution on articular surfaces: application to joint stability analysis. Journal of Biomechanics 23 (1990) 1013–20.

[57] W. Goldsmith. Impact, the Theory and Physical Behaviour of Colliding Solids, Edward Arnold Ltd., 1960.

[58] G. Gilardi, I. Sharf. Literature survey of contact dynamics modelling. Mechanism and Machine Theory 37 (2002) 1213–1239

[59] J. Alves, N. Peixinho, M. Tavares da Silva, P. Flores, H.L. Lankarani, A comparative study of the viscoelastic constitutive models for frictionless contact interfaces in solids. Mechanism and Machine Theory 85 (2015) 172–188.

[60] D.W. Marhefka, D.E. Orin, A compliant contact model with nonlinear damping for simulation of robotic systems, IEEE Trans. Syst. Man Cybern. Syst. Hum. 29 (1999) 566–572.

[61] R.G. Herbert, D.C. McWhannell, Shape and frequency composition of pulses from an impact pair, J. Eng. Ind. 99 (1977) 513–518.

[62] T.W. Lee, A.C. Wang, On the dynamics of intermittent-motion mechanisms. Part 1: dynamic model and response, J. Mech. Transm. Autom. Des. 105 (1983) 534–540.

[63] Y. Gonthier, J. McPhee, C. Lange, J.C. Piedboeuf, A regularized contact model with asymmetric damping and dwell-time dependent friction,Multibody Syst. Dyn. 11 (2004) 209–233.

[64] Y. Zhang, I. Sharf, Compliant forcemodeling for impact analysis, Proceedings of the 2004 ASME International Design Technical Conferences, Salt Lake City, Paper No. DETC2004–572202004.

[65] Q. Zhiying, L. Qishao, Analysis of impact process based on restitution coefficient, J. Dyn. Control 4 (2006) 294-298.

[66] M. Gharib, Y. Hurmuzlu, A new contact force model for low coefficient of restitution impact, J. Appl. Mech. 79 (6) (2012) 064506.

[67] E. Askari, P. Flores, D. Dabirrahmani, R. Appleyard, A computational analysis of squeaking hip prostheses. ASME J. Comput. Nonlinear Dyn. 10(2) (2015)

[68] K.A. Atkinson, An Introduction to Numerical Analysis, 2nd edn. Wiley, New York (1989).

[69] G. Bergmann, G., Deuretzbacher, M. Heller, F. Graichen, A. Rohlmann, J. Strauss, et al.: Hip contact forces and gait patterns from routine activities. J. Biomech. 34(7) (2001)) 859–871.

[70] L. Kang, A.L. Galvin, Z.M. Jin, et al. A simple fully integrated contact-coupled wear prediction for ultra-high molecular weight polyethylene hip implants. ProcIMechE, Part H: J Engineering in Medicine 220 (2006) 33-46.